

Spin-tensor–momentum-coupled Bose-Einstein condensates

Xi-Wang Luo, Kuei Sun, and Chuanwei Zhang*

Department of Physics, The University of Texas at Dallas, Richardson, Texas 75080-3021, USA

The recent experimental realization of spin-orbit coupling for ultracold atomic gases provides a powerful platform for exploring many interesting quantum phenomena. In these studies, spin represents spin vector (spin-1/2 or spin-1) and orbit represents linear momentum. Here we propose a scheme to realize a new type of spin-tensor–momentum coupling (STMC) in spin-1 ultracold atomic gases. We study the ground state properties of interacting Bose-Einstein condensates (BECs) with STMC and find interesting new types of stripe superfluid phases and multicritical points for phase transitions. Furthermore, we show that a stripe phase with a long tunable period and high visibility of density modulation can be dynamically generated using STMC, paving the way for direct experimental observation of the long-sought stripe phases. Our scheme for generating STMC can be generalized to other systems and may open the door for exploring novel quantum physics and device applications.

Introduction. The coupling between matter and gauge field plays a crucial role for many fundamental quantum phenomena and practical device applications in condensed matter [1–3] and atomic physics [4]. A prominent example is the spin-orbit coupling, the coupling between a particle’s spin and orbit (e.g., momentum) degrees of freedom, which is responsible for important physics such topological insulators and superconductors [2, 3]. In this context, recent experimental realization of spin-orbit coupling in ultracold atomic gases [5–13] opens a completely new avenue for investigating quantum many-body physics under gauge field [14–28].

So far in most works on spin-orbit coupling in solid state and cold atomic systems, the spin degrees of freedom are taken as rank-1 spin vectors F_i ($i = x, y, z$), such as electron spin-1/2 or pseudospins formed by atomic hyperfine states that can be large (e.g., spin-1 or 3/2). Experimentally, spin-orbit coupling for spin-1 Bose-Einstein condensates (BECs) has been realized recently [29, 30] and interesting magnetism physics has been observed [31–35]. Mathematically, it is well known that there exist not only spin vectors, but also spin tensors [e.g., irreducible rank-2 spin-quadrupole tensor $N_{ij} = (F_i F_j + F_j F_i)/2 - \delta_{ij} \mathbf{F}^2/3$] in a large spin (≥ 1) system. Therefore two natural questions are: *i*) Can the coupling between spin tensors of particles and their linear momenta be realized in experiments? *ii*) What new physics may emerge from such spin-tensor–momentum coupling (STMC)?

In this Letter, we address these two questions by proposing a simple experimental scheme for realizing STMC for spin-1 ultracold atomic gases. Our scheme is based on slight modification of previous experimental setup [29] and is experimentally feasible. The STMC changes the band structure dramatically, leading to interesting new physics in the presence of many-body interactions between atoms. Although both bosons and fermions can be studied, here we only consider spin-1 BECs to illustrate the effects of STMC. Our main results are:

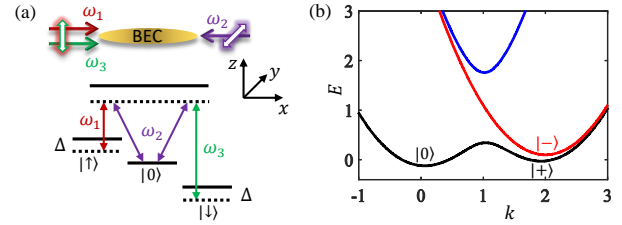


FIG. 1: (a) Top: Experimental scheme to generate STMC in BEC. Bottom: Raman transitions between three hyperfine spin states with detuning Δ . (b) Single-particle band structure for Raman strength $\Omega = 0.5$ and detuning $\Delta = 0.1$. The (dominant) spin components $|0\rangle$ and $|\pm\rangle = \frac{1}{\sqrt{2}}(|\uparrow\rangle \pm |\downarrow\rangle)$ are indicated around the corresponding band minima.

i) The single particle band structure with STMC consists of two bright-state bands (top and bottom) and one dark-state middle band [Fig. 1(b)], where the dark-state band is not coupled with two bright-state bands through Raman coupling. However, the dark-state band plays an important role on both ground-state and dynamical properties of the BEC in the presence of interactions.

ii) We study the ground-state phase diagrams with exotic plane-wave and stripe phases, where the dark-state middle band can be partially populated despite not the single particle ground state. The transitions between different phases possess interesting multicriticality phenomena with triple, quadruple, and even quintuple points.

iii) The existence of dark middle band makes it possible to generate a stripe phase with a long tunable period and high visibility of density modulations, which may be directly measured in experiments. The stripe state is a coherent superposition of two or more plane-wave states and possesses both superfluid and crystalline properties, resembling supersolids [36]. Recently, the stripe phase has been experimentally observed indirectly using Bragg reflection [37]. Generally, the density modulations of stripe phases have a short period and low visibility [38], therefore a direct real space measurement of stripe patterns is still challenging. Utilizing the dark middle

band from STMC, we show that a stripe state with a long tunable period ($\sim 5\mu\text{m}$) and high visibility ($\sim 100\%$) can be dynamically generated with realistic experimental parameters.

The model. We consider a setup similar as that in the recent experiment [29] but with a slightly different laser configuration, as shown in Fig. 1(a), where three Raman lasers with wavenumber k_R are employed to generate STMC. The three lasers induce two Raman transitions between hyperfine spin states $|0\rangle$ and $|\uparrow(\downarrow)\rangle$, both of which have the same recoil momentum $2k_R$ along the x direction. The single-particle Hamiltonian in the spin-1 basis ($|\uparrow\rangle, |0\rangle, |\downarrow\rangle$)^T is (we set $\hbar = 1$)

$$\tilde{H}_0 = -\frac{\nabla^2}{2m} + \Delta F_z^2 + \left(\sqrt{2}\Omega e^{i2k_R x} |0\rangle\langle +| + h.c. \right), \quad (1)$$

where $F_z^2 = |\uparrow\rangle\langle +| + |\downarrow\rangle\langle -|$ is equivalent to the spin tensor N_{zz} (up to a constant), $|+\rangle \equiv \frac{1}{\sqrt{2}}(|\uparrow\rangle + |\downarrow\rangle)$, Ω is the Raman coupling strength, and Δ is the detuning for both $|\uparrow\rangle$ and $|\downarrow\rangle$ states. We see that another spin state $|- \rangle \equiv \frac{1}{\sqrt{2}}(|\uparrow\rangle - |\downarrow\rangle)$ is always an eigenstate and does not couple to $|0\rangle$ nor $|+\rangle$ through Ω , and thus is a dark state.

Since the BEC wavefunction in the y and z directions is not affected by the Raman lasers, we can consider the physics only along the x direction [33–35]. After a unitary transformation $U = \exp(-i2k_R x F_z^2)$ to quasi-momentum basis, we write the Hamiltonian in energy and momentum units $\frac{k_R^2}{2m}$ and k_R , respectively, as

$$H_0 = -\partial_x^2 + (\Delta + 4 + 4i\partial_x)F_z^2 + \sqrt{2}\Omega F_x, \quad (2)$$

where Ω and Δ are dimensionless transverse-Zeeman and spin-tensor potential, respectively, and $(i\partial_x)F_z^2$ describes the coupling between spin tensor F_z^2 and the linear momentum, *i.e.*, STMC.

The single-particle Hamiltonian has three energy bands [see a typical structure in Fig. 1(b)]. The dark-state middle band always has the spin state $|- \rangle$ and spectrum $(k-2)^2 + \Delta$, which are independent of Ω . Without the middle band, we find the top and bottom bright-state bands exhibit the same physics as the known spin-orbit-coupled spin-1/2 system: the two spin branches $|0\rangle$ and $|+\rangle$ with relative energy difference Δ are separated by $2k_R$ at $\Omega = 0$, and mixed to form top/bottom bands with a gap at a finite Ω . At $\Delta = 0$, the bottom band has degenerate double minima for $\Omega < \sqrt{2}E_R$, above which the band makes a transition to a single-minimum structure. The decoupling of the middle band is protected by the spin-tensor symmetry $[F_x^2, H_0] = 0$, under which the middle band (top and bottom bands) corresponds to $\langle F_x^2 \rangle = 0$ (1). Therefore, even if the gap between the middle and bottom band minima is small [$\sim O(\Omega^2)$ at weak Ω], the single-particle ground state always selects the bottom band. However, the atomic interactions can break the symmetry and drastically change the BEC's

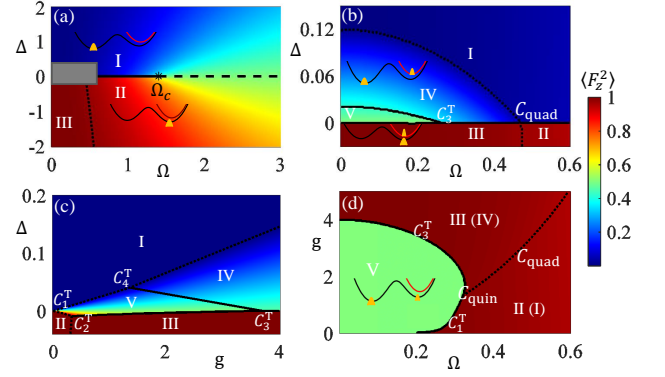


FIG. 2: (a) Ground state phase diagram in the Ω - Δ plane with $g\bar{n} = 3$. The dashed line is a crossover boundary. (b) Zoom in of the framed region in (a). (c) [(d)] Ground state phase diagram in the g - Δ (g - Ω) plane with $\Omega = 0.16$ ($\Delta = 0$). Solid (dotted) lines represent first (second) order phase transitions. The interaction ratio is $g_0 = -50g_2 \equiv g$.

ground state as well as dynamical properties by involving the middle band.

Under the Gross-Pitaevskii (GP) mean-field approximation, the energy density becomes

$$\varepsilon = \frac{1}{V} \int dx \left[\Psi^\dagger H_0 \Psi + \frac{g_0}{2} (\Psi^\dagger \Psi)^2 + \frac{g_2}{2} (\Psi^\dagger \mathbf{F}_U \Psi)^2 \right], \quad (3)$$

where V is the system volume, $\mathbf{F}_U = U^\dagger \mathbf{F} U$ is the unitarily transformed spin operator, and Ψ is the three-component condensate wavefunction normalized by the average particle number density $\bar{n} = V^{-1} \int dx \Psi^\dagger \Psi$. The interaction strengths $g_{0,2}$ represent density and spin interactions in spinor condensates [39, 40], respectively. Since U is a spatially dependent spin tensor, the x and y components of \mathbf{F}_U exhibit spatial modulation that cannot be eliminated through any local spin rotation (different from previous models [33–35]). Such modulation is essential for stripe phases in the system.

We consider a variational ansatz [41]

$$\Psi = \sqrt{\bar{n}} (|c_1| \chi_1 e^{ik_1 x} + |c_2| \chi_2 e^{ik_2 x + i\alpha}) \quad (4)$$

to find the ground state, with spinors $\chi_j = (\cos \theta_j \cos \phi_j, -\sin \theta_j, \cos \theta_j \sin \phi_j)^T$, and the normalization condition $|c_1|^2 + |c_2|^2 = 1$. The energy density now becomes a functional of eight variational parameters $|c_1|$, k_1 , k_2 , θ_1 , θ_2 , ϕ_1 , ϕ_2 , and α , and its minimization leads to the ground state [41]. The quantum phase diagram can be characterized with the variational wavefunction, experimental observables $\langle F_z \rangle$ and $\langle F_z^2 \rangle$, and the symmetry property $\langle F_x^2 \rangle$. We also numerically solve the GP equation using imaginary time evolution to obtain the ground states, which are in good agreement with the variational results.

Phase diagram. For ferromagnetic interaction $g_2 < 0$ (e.g., ^{87}Rb), the BEC has three plane-wave ($|c_1 c_2| = 0$)

and two stripe ($|c_1 c_2| \neq 0$) phases (Fig. 2): (I) plane-wave phase in $k < 1$, having $\langle F_z \rangle = 0$ (spin unpolarized), $\langle F_z^2 \rangle < 0.5$, and $\langle F_x^2 \rangle = 1$ (middle band unpopulated); (II) plane-wave phase in $k > 1$, having $\langle F_z \rangle = 0$, $\langle F_z^2 \rangle > 0.5$, and $\langle F_x^2 \rangle = 1$; (III) spin-polarized plane-wave phase in $k > 1$ having $\langle F_z \rangle \neq 0$ and $\langle F_x^2 \rangle < 1$ (middle band populated); (IV) mix-band stripe phase, having $k_1 < 1$, $k_2 > 1$, and $\langle F_x^2 \rangle < 1$; (V) bottom-band stripe phase, same as (IV) except $\langle F_x^2 \rangle = 1$. The last three phases exhibit Z_2 ferromagnetism: phases (III), (IV), and (V) all have twofold degenerate ground states with global ferromagnetic order $\pm \langle F_z \rangle \neq 0$, $\pm \langle F_y \rangle \neq 0$, and $\pm \langle F_x \rangle \neq 0$, respectively. Note that these orders are calculated in the laboratory frame (the basis of \hat{H}_0) and reflect the energetic favor by the ferromagnetic interaction. For anti-ferromagnetic interaction $g_2 > 0$ (e.g., ^{23}Na), the system has a relatively simple phase diagram containing only two plane-wave phases (I) and (II), separated by a first-order phase-boundary at $\Delta = 0$. Hereafter we focus on the ferromagnetic case.

In Fig. 2(a) we plot the phase diagram in the Ω - Δ plane. At a sufficiently large Ω , the middle band does not participate in the ground state, so the phase diagram is similar to the spin-orbit-coupled spin-1/2 system: the two plane-wave phases (I) and (II) are separated by a first-order-transition boundary (solid line along $\Delta = 0$) if $\Omega < \Omega_c$ or a crossover one (dashed line) if $\Omega > \Omega_c$. As Ω decreases, the middle band minimum gets closer to the right minimum of the bottom band [Fig. 1(b)]. If the BEC originally stays in the plane-wave phase (II) ($\Delta < 0$), it starts to partially occupy the middle band [Fig. 2(b), bottom inset], undergoing a second-order transition (dotted curve) to the polarized phase (III). From the energetic point of view, the BEC populates to a slightly higher single particle energy state to get polarized to reduce ferromagnetic interaction energy. Note that phase (III) is still a plane-wave phase since the BEC occupies both bands at the same k .

At a small Ω and $\Delta > 0$, the energy difference between the single-particle band minimum [plane wave (I)] and the other bottom-band minimum [plane wave (II)] or the middle-band minimum is comparable to the interaction energy, so the BEC may favor the co-occupation of (I) and a higher-energy local minimum as long as the total energy can be reduced more by the interaction. In Fig. 2(b), we zoom in the framed region of Fig. 2(a) and show the emergence of two stripe phases. The mix-band stripe phase (IV) is the superposition of plane wave (I) and the one around the middle-band minimum (top inset). Phase (IV) exhibits spin-density waves due to the superposition [Fig. 3(a)] and a global ferromagnetic order $\langle F_y \rangle \neq 0$ that reduces the g_2 interaction energy, compensating the higher middle-band energy. Note that phase (IV) has a uniform total density due to the orthogonality between the middle and bottom band spins, but the spin-density waves form a stripe pattern. The bottom-band

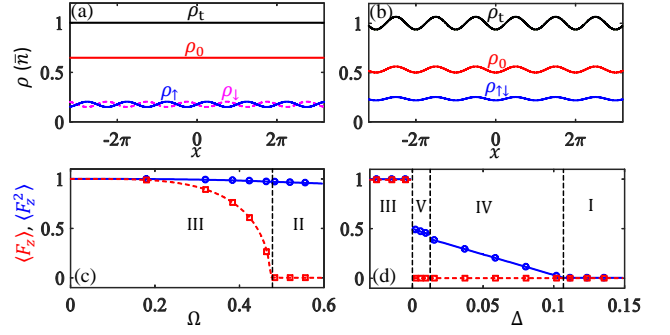


FIG. 3: (a) [(b)] The local density modulations of phase (IV) [(V)] in Fig. 2(b), with $\Omega = 0.16$ and $\Delta = 0.006$ ($\Delta = 0.023$). (c) [(d)] $\langle F_z^2 \rangle$ (solid line) and $\langle F_z \rangle$ (dashed line) vs Ω (Δ) along the path $\Delta = -0.018$ ($\Omega = 0.16$) in Fig. 2(b). Dots (lines) are obtained from imaginary time GP equation (variational method).

stripe phase (V), which appears at even weaker Ω and Δ , is the superposition of two bottom-band plane waves (I) and (III) [Fig. 2(d) inset]. Phase (V) exhibits a total-density wave [Fig. 3(b)], which, compared with (IV), increases the g_0 interaction energy, but the total energy is favorable due to the pure bottom-band occupation and global ferromagnetic order $\langle F_x \rangle \neq 0$. We remark that the superposition of three plane waves (with co-occupation of three band minima) is never energetically favorable because it cannot maximize the ferromagnetic order.

Returning to the phase diagram Fig. 2(b), the (I)–(IV) phase boundary corresponds to a second-order transition, which meets the (II)–(III) boundary at a quadruple point C_{quad} at $\Delta = 0$. The (IV)–(V) boundary corresponds to a first-order transition, which encounters phase (III) at a triple point C_3^T at $\Delta = 0$. To study the dependence on interaction, we plot the phase diagram in the Δ - g plane in Fig. 2(c), with a fixed ratio $g_0 = -50g_2 \equiv g$. We see that the stripe region increases with g (due to the increasing g_2), and phase (IV) is more favorable than (V) in the large- g region (due to the large g_0). For the plane-wave phases (II) and (III), the latter has global ferromagnetic order $\langle F_z \rangle \neq 0$ and is hence favorable with strong interaction. The Δ - g diagram also shows first-order transitions between any two of (III), (IV), and (V) phases, second-order transitions between any other adjacent phases, and four triple points $C_{1,2,3,4}^T$ at the (I)–(II)–(V), (II)–(III)–(V), (III)–(IV)–(V), and (I)–(IV)–(V) encounters, respectively. In Fig. 2(d), we show how the encounters of phases along $\Delta = 0$ change with the interaction. We see that phases (III) and (IV) survive at large g , while (I) and (II) survive at large Ω , in agreement with the energetic argument. The boundaries represent three traces of triple points $C_{1,3}^T$ and quadruple point C_{quad} , respectively, which intercept at a quintuple point C_{quin} as the joint of all five phases.

In Figs. 3(a) and (b), we plot spatial profiles of each

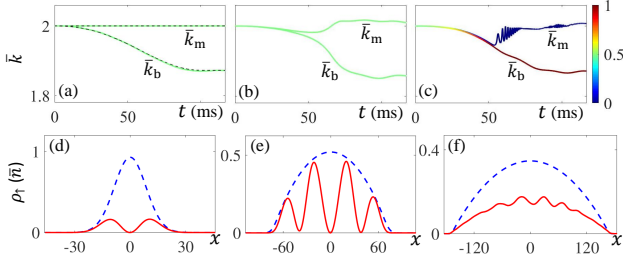


FIG. 4: (a)-(c) Averaged momentum \bar{k}_m (\bar{k}_b) and percent-age population (colorbar) of atoms in the middle (bottom) band. Thin dashed line in (a) shows the band minima. (d)-(f) The initial (dashed line) and final (solid line) spin density ρ_t corresponding to (a)-(c) respectively. The interactions are $(g_0\bar{n}, g_2\bar{n}) = (0, 0)$, $(0.5, 0)$ and $(4, -0.2)$ for (a), (b) and (c). Other parameters are $T = 100\text{ms}$, $\Delta = -0.05$, and $\Omega_f = 0.7$.

spin component's density $\rho_{\downarrow,0,\uparrow}$ and total density ρ_t for stripe phases (IV) and (V), respectively. Phase (IV) shows out-of-phase modulations between ρ_{\uparrow} and ρ_{\downarrow} , representing spin-vector (F_z) density wave, and uniform ρ_0 and ρ_t , while (V) shows in-phase modulations of all components and hence ρ_t , of which $\rho_{\uparrow,\downarrow}$ overlap each other, representing spin-tensor (F_z^2) density wave. The modulation wavelength matches the laser's recoil momentum $2k_R$, i.e., the momentum difference between the two plane waves is $|k_2 - k_1| = 2k_R$. This can be understood in the quasi-momentum frame that the minimization of g_2 interaction requires equal modulations between the spin components and the spin operator \mathbf{F}_U in Eq. (3). Since the separation between two band minima is smaller than $2k_R$ at finite Ω , the two plane-wave components of the stripe phases do not exactly stay on the band minima. Previously, $\langle F_z \rangle$ and $\langle F_z^2 \rangle$ have been used in experiments [29] for characterizing phase transitions. In Figs. 3(c) and (d), we plot $\langle F_z \rangle$ (squares) and $\langle F_z^2 \rangle$ (circles) along (III)-(II) and (III)-(V)-(IV)-(I) transition paths in Fig. 2(b), respectively. The discontinuity in spin-tensor polarization $\langle F_z^2 \rangle$ (its first derivative) indicates the occurrence of first-order (second-order) phase transition.

Dynamical stripe state. The middle-band minimum and the right bottom-band minimum are both near $k = 2$ and close to each other. Therefore a coherent superposition of plane waves on these two minima leads to a long-period stripe state, which can be directly measured in experiments. To generate such a stripe state, we consider ^{87}Rb atoms in a harmonic trap $\omega = 2\pi \times 50\text{Hz}$, initially prepared in spin state $|\uparrow\rangle$ with the Raman lasers off. The two minima coincide and are equally populated as $|\uparrow\rangle = \frac{1}{\sqrt{2}}(|+\rangle + |-\rangle)$. The 800-nm Raman lasers are gradually turned on such that Ω increases from 0 to Ω_f within a time T and then remains constant. The two equally populated plane waves are expected to slightly split, leading to the stripe state.

We start by considering the non-interacting atoms, and calculate the final state by solving the real-time GP equa-

tion. For $\omega T \gg 1$, atoms in the middle and bottom bands follow their minima respectively and their wave packages split in the momentum space. The final state is a stripe state similar to phase (IV), except that the stripe pattern is moving rather than stationary due to the dynamical phases of the two bands [41]. Compared to phase (IV), the dynamical stripe state has a higher visibility and a longer period, and thus easier for direct observations in experiments. The evolution of averaged momentum \bar{k}_b (\bar{k}_m) of atoms in the bottom (middle) band and the final stripe patterns are shown in Figs. 4(a) and (d). We see that \bar{k}_m remains unchanged since the middle band is independent of Ω , and \bar{k}_b follows closely the bottom-band minimum, with slight dipole oscillation [42] at $t > T$ due to the collective excitations caused by the finite increasing rate of Ω .

The system undergoes different dynamic processes when interactions are included. In general $|g_2| \ll g_0$, and for weakly interacting BECs, we first focus on the density-interaction effects and neglect the spin interaction. The density interaction g_0 preserves the spin states and thus the atom populations of the two bands remain unchanged. However, the momentum of atoms in the middle band is no longer conserved due to the interaction. We find that \bar{k}_m shifts together with \bar{k}_b at the beginning then they separate and eventually return to their band minima respectively. At $t > T$, the density interaction induces synchronous dipole oscillations of \bar{k}_m and \bar{k}_b with a frequency different from the single-particle case [see Fig. 4(b)]. Nevertheless, we obtain a stripe state as the final state [see Fig. 4(e)] with a long period ($\sim 5\mu\text{m}$ for $\Omega_f = 0.7$) and high visibility (close to 100%). For ^{87}Rb with $g_2 = -0.005g_0$, such dynamical stripe states can always be obtained in the weakly interacting region where $|g_2|\bar{n} \ll T^{-1}$ [41]. Also, the stripe period can be tuned by changing the value of Ω_f (e.g. $\Omega_f = 1$ leads to a period of $\sim 3\mu\text{m}$) [41]. In the strongly interacting region, the spin interaction scatters atoms from the middle to bottom band as Ω increases, and its effects cannot be neglected when the spin interaction is strong compared to T^{-1} . In this case, the final state has no middle-band population and no stripe states would be obtained, i.e., increasing Ω drives the system from phase (III) to phase (II). Figs. 4(c) and (f) show our numerical results with tiny stripes caused by weak excitations.

Conclusions. In summary, we propose a scheme to realize STMC in a spin-1 BEC, and study its ground-state and dynamical properties. The interplay between STMC and atomic interactions leads to many interesting quantum phases and multicritical points for phase transitions. The STMC offers a simple way to generate stripe states with high visibility and long tunable periods, paving the way for direct experimental observation of long-sought stripe states. The proposed STMC for ultracold atoms open the door for exploring many other interesting physics, such as STMC fermionic su-

perfluids, Bogoliubov excitations with interesting roton spectrum [43, 44], non-Abelian STMC (similar as Rashba spin-orbit coupling), *etc.*

Acknowledgements: We thank P. Engels for helpful discussion. This work is supported by AFOSR (FA9550-16-1-0387), NSF (PHY-1505496), and ARO (W911NF-17-1-0128).

* Corresponding author.

Email: chuanwei.zhang@utdallas.edu

- [1] D. Xiao, M.-C. Chang, and Q. Niu, Berry phase effects on electronic properties, *Rev. Mod. Phys.* **82**, 1959, (2010).
- [2] M. Hasan and C. Kane, Colloquium: topological insulators, *Rev. Mod. Phys.* **82**, 3045, (2010).
- [3] X.-L. Qi and S.-C. Zhang, Topological insulators and superconductors, *Rev. Mod. Phys.* **83**, 1057, (2011).
- [4] J. Dalibard, F. Gerbier, G. Juzeliūnas, and P. Öhberg, Colloquium: Artificial gauge potentials for neutral atoms, *Rev. Mod. Phys.* **83**, 1523, (2011).
- [5] Y.-J. Lin, K. Jiménez-García, and I. B. Spielman, Spin-orbit-coupled bose-einstein condensates, *Nature (London)* **471**, 83, (2011).
- [6] J.-Y. Zhang, *et al.*, Collective dipole oscillations of a spin-orbit coupled bose-einstein condensate, *Phys. Rev. Lett.* **109**, 115301, (2012).
- [7] C. Qu, C. Hamner, M. Gong, C. Zhang, and P. Engels, Observation of zitterbewegung in a spin-orbit-coupled bose-einstein condensate, *Phys. Rev. A* **88**, 021604, (2013).
- [8] A. Olson, S. Wang, R. Niffenegger, C. Li, C. Greene, and Y. Chen, Tunable landau-zener transitions in a spin-orbit-coupled bose-einstein condensate, *Phys. Rev. A* **90**, 013616, (2014).
- [9] P. Wang, *et al.*, Spin-orbit coupled degenerate fermi gases, *Phys. Rev. Lett.* **109**, 095301, (2012).
- [10] L. Cheuk, A. Sommer, Z. Hadzibabic, T. Yefsah, W. Bakr, and M. Zwierlein, Spin-injection spectroscopy of a spin-orbit coupled fermi gas, *Phys. Rev. Lett.* **109**, 095302, (2012).
- [11] R. A. Williams, M. C. Beeler, L. J. LeBlanc, K. Jiménez-García, and I. B. Spielman, Raman-Induced Interactions in a Single-Component Fermi Gas Near an *s*-Wave Feshbach Resonance, *Phys. Rev. Lett.* **111**, 095301 (2013).
- [12] L. Huang, *et al.*, Experimental realization of two-dimensional synthetic spin-orbit coupling in ultracold fermi gases, *Nature Phys.* **12**, 540, (2016).
- [13] Z. Wu, *et al.*, Realization of two-dimensional spin-orbit coupling for bose-einstein condensates, *Science* **354**, 83, (2016).
- [14] T. D. Stanescu, B. Anderson, and V. Galitski, Spin-orbit coupled Bose-Einstein condensates, *Phys. Rev. A* **78**, 023616 (2008).
- [15] C. Zhang, S. Tewari, R. Lutchyn, and S. Das Sarma, $p_x + ip_y$ superfluid from *s*-wave interactions of fermionic cold atoms, *Phys. Rev. Lett.* **101**, 160401, (2008).
- [16] C. Wu, I. Mondragon-Shem, and X.-F. Zhou, Unconventional Bose-Einstein Condensations from Spin-Orbit Coupling, *Chin. Phys. Lett.* **28**, 097102 (2011).
- [17] C. Wang, C. Gao, C. Jian, and H. Zhai, Spin-orbit coupled spinor bose-einstein condensates, *Phys. Rev. Lett.* **105**, 160403, (2010).
- [18] T.-L. Ho and S. Zhang, Bose-einstein condensates with spin-orbit interaction, *Phys. Rev. Lett.* **107**, 150403, (2011).
- [19] Y. Li, L. Pitaevskii, and S. Stringari, Quantum tricriticality and phase transitions in spin-orbit coupled bose-einstein condensates, *Phys. Rev. Lett.* **108**, 225301, (2012).
- [20] Y. Zhang, L. Mao, and C. Zhang, Mean-field dynamics of spin-orbit coupled bose-einstein condensates, *Phys. Rev. Lett.* **108**, 035302, (2012).
- [21] H. Hu, B. Ramachandran, H. Pu, and X. Liu, Spin-orbit coupled weakly interacting bose-einstein condensates in harmonic traps, *Phys. Rev. Lett.* **108**, 010402, (2012).
- [22] T. Ozawa and G. Baym, Stability of ultracold atomic bose condensates with rashba spin-orbit coupling against quantum and thermal fluctuations, *Phys. Rev. Lett.* **109**, 025301, (2012).
- [23] M. Gong, S. Tewari, and C. Zhang, BCS-BEC Crossover and Topological Phase Transition in 3D Spin-Orbit Coupled Degenerate Fermi Gases, *Phys. Rev. Lett.* **107**, 195303 (2011).
- [24] H. Hu, L. Jiang, X.-J. Liu, and H. Pu, Probing Anisotropic Superfluidity in Atomic Fermi Gases with Rashba Spin-Orbit Coupling, *Phys. Rev. Lett.* **107**, 195304 (2011).
- [25] Z.-Q. Yu and H. Zhai, Spin-Orbit Coupled Fermi Gases across a Feshbach Resonance, *Phys. Rev. Lett.* **107**, 195305 (2011).
- [26] C. Qu, Z. Zheng, M. Gong, Y. Xu, L. Mao, X. Zou, G. Guo, and C. Zhang, Topological superfluids with finite-momentum pairing and Majorana fermions, *Nat. Commun.* **4**, 2710 (2013).
- [27] W. Zhang and W. Yi, Topological Fulde-Ferrell-Larkin-Ovchinnikov states in spin-orbit-coupled Fermi gases, *Nat. Commun.* **4**, 2711 (2013).
- [28] V. Galitski and I. B. Spielman, Spin-orbit coupling in quantum gases, *Nature (London)* **494**, 49, (2013).
- [29] D. Campbell, R. Price, A. Putra, A. Valdés-Curiel, D. Trypogeorgos, and I. B. Spielman, Magnetic phases of spin-1 spin-orbit-coupled Bose gases, *Nat. Commun.* **7**, 10897 (2016).
- [30] X. Luo, *et al.*, Tunable atomic spin-orbit coupling synthesized with a modulating gradient magnetic field, *Sci. Rep.* **6**, 18983, (2016).
- [31] Z. Lan and P. Öhberg, Raman-dressed spin-1 spin-orbit-coupled quantum gas, *Phys. Rev. A* **89**, 023630, (2014).
- [32] S. S. Natu, X. Li, and W. S. Cole, Striped ferronematic ground states in a spin-orbit-coupled $S = 1$ Bose gas, *Phys. Rev. A* **91**, 023608, (2015).
- [33] K. Sun, C. Qu, Y. Xu, Y. Zhang, and C. Zhang, Interacting spin-orbit-coupled spin-1 bose-einstein condensates, *Phys. Rev. A* **93**, 023615, (2016).
- [34] Z.-Q. Yu, Phase transitions and elementary excitations in spin-1 Bose gases with Raman-induced spin-orbit coupling, *Phys. Rev. A* **93**, 033648, (2016).
- [35] G. Martone, F. Pepe, P. Facchi, S. Pascazio, and S. Stringari, Tricriticalities and quantum phases in spin-orbit-coupled spin-1 bose gases, *Phys. Rev. Lett.* **117**, 125301, (2016).
- [36] Y. Pomeau and S. Rica, Dynamics of a model of super-solid, *Phys. Rev. Lett.* **72**, 2426, (1994).

- [37] J. Li, *et al.*, A stripe phase with supersolid properties in spin-orbit-coupled bose-einstein condensates, *Nature (London)* **543**, 91, (2017).
- [38] G. Martone, Y. Li, and S. Stringari, Approach for making visible and stable stripes in a spin-orbit-coupled Bose-Einstein superfluid, *Phys. Rev. A* **90**, 041604(R) (2014).
- [39] T.-L. Ho, Spinor bose condensates in optical traps, *Phys. Rev. Lett.* **81**, 742, (1998).
- [40] T. Ohmi and K. Machida, Bose-Einstein condensation with internal degrees of freedom in alkali atom gases, *J. Phys. Soc. Jpn.* **67**, 1822 (1998).
- [41] Supplementary materials, *See supplementary materials for details.*
- [42] Z. Chen and H. Zhai, Collective-mode dynamics in a spin-orbit-coupled bose-einstein condensate, *Phys. Rev. A* **86**, 041604, (2012).
- [43] M. Khamsehchi, Y. Zhang, C. Hamner, T. Busch, and P. Engels, Measurement of collective excitations in a spin-orbit-coupled bose-einstein condensate, *Phys. Rev. A* **90**, 063624, (2014).
- [44] S.-C. Ji, L. Zhang, X.-T. Xu, Z. Wu, Y. Deng, S. Chen, and J.-W. Pan, Softening of Roton and Phonon Modes in a Bose-Einstein Condensate with Spin-Orbit Coupling, *Phys. Rev. Lett.* **114**, 105301 (2015).

Supplementary Materials

Validation of the ansatz

The ground state is mainly determined by the two lower bands, with three minima in total. We may consider a more general ansatz

$$\Psi = \sqrt{\bar{n}} (|c_1|\chi_1 e^{ik_1 x} + |c_2|\chi_2 e^{ik_2 x + i\alpha} + |c_3|\chi_3 e^{ik_3 x + i\beta}), \quad (\text{S1})$$

with $k_1 \simeq 0$, $k_{2,3} \simeq 2$, and $\chi_i = (\cos \theta_i \cos \phi_i, -\sin \theta_i, \cos \theta_i \sin \phi_i)^T$. The stripe phase is supposed to lower the spin interaction $g_2(\Psi^\dagger \mathbf{F}_U \Psi)^2$ by generating ferromagnetic order. The ferromagnetic order is maximized when $k_2 = k_3 = k_1 + 2$, that is when the modulation of the spin density is equal to the modulation of the spin operator \mathbf{F}_U . Then Eq. (S1) is reduced to the ansatz given in the main text. The above arguments are verified numerically by considering the ansatz Eq. (S1) and we always have $k_3 = k_2 = k_1 + 2$ for the ground state.

Variational energy density

In the following, we give a detailed derivation of the variational energy density, using the variational ansatz

$$\Psi = \begin{pmatrix} \psi_{+1} \\ \psi_0 \\ \psi_{-1} \end{pmatrix} = \sqrt{\bar{n}}|c_1| \begin{pmatrix} \cos(\theta_1) \cos(\phi_1) \\ -\sin(\theta_1) \\ \cos(\theta_1) \sin(\phi_1) \end{pmatrix} e^{ik_1 x} + \sqrt{\bar{n}}|c_2| \begin{pmatrix} \cos(\theta_2) \cos(\phi_2) \\ -\sin(\theta_2) \\ \cos(\theta_2) \sin(\phi_2) \end{pmatrix} e^{ik_2 x + i\alpha}. \quad (\text{S2})$$

The single particle energy density is

$$\varepsilon_0 = \frac{1}{V} \int \Psi^\dagger H_0 \Psi dx = \frac{1}{V} \int \Psi^\dagger [(-\partial_x^2) + (\Delta + 4 + 4i\partial_x)F_z^2 + \sqrt{2}\Omega F_x] \Psi dx. \quad (\text{S3})$$

We have

$$\frac{1}{V} \int \Psi^\dagger (-\partial_x^2) \Psi dx = \frac{1}{V} \int \sum_{j=0,\pm 1} \psi_j^* (-\partial_x^2) \psi_j dx = \bar{n} \sum_{i=1}^2 |c_i|^2 k_i^2, \quad (\text{S4})$$

similarly we can obtain

$$\frac{1}{V} \int \Psi^\dagger \sqrt{2}\Omega F_x \Psi dx = -\bar{n}\sqrt{2}\Omega \sum_{i=1}^2 |c_i|^2 \sin(2\theta_i) \sin(\phi_i + \frac{\pi}{4}), \quad (\text{S5})$$

and

$$\frac{1}{V} \int \Psi^\dagger (\Delta + 4 + 4i\partial_x) F_z^2 \Psi dx = \bar{n} \sum_{i=1}^2 (\Delta + 4 - 4k_i) |c_i|^2 \cos^2(\theta_i). \quad (\text{S6})$$

The density-interaction energy is

$$\begin{aligned}\varepsilon_d &= \frac{1}{V} \int dx \frac{g_0}{2} (\Psi^\dagger \Psi)^2 = \frac{g_0}{2} \frac{1}{V} \int dx \left(\sum_{j=0, \pm 1} |\psi_j|^2 \right)^2 \\ &= \bar{n} \frac{g_0 \bar{n}}{2} \{1 + 2|c_1|^2 |c_2|^2 [\sin(\theta_1) \sin(\theta_2) + \cos(\theta_1) \cos(\theta_2) \cos(\phi_1 - \phi_2)]^2\},\end{aligned}\quad (\text{S7})$$

and the spin-interaction energy is

$$\varepsilon_s = \frac{1}{V} \int dx \frac{g_2}{2} (\Psi^\dagger \mathbf{F}_U \Psi)^2, \quad (\text{S8})$$

with spatially modulated spin operator $\mathbf{F}_U = (F_U^x, F_U^y, F_U^z)$,

$$F_U^x = \frac{1}{\sqrt{2}} \begin{pmatrix} 0 & e^{i2k_R x} & 0 \\ e^{-i2k_R x} & 0 & e^{-i2k_R x} \\ 0 & e^{i2k_R x} & 0 \end{pmatrix} \quad (\text{S9})$$

$$F_U^y = \frac{1}{\sqrt{2}} \begin{pmatrix} 0 & -ie^{i2k_R x} & 0 \\ ie^{-i2k_R x} & 0 & -ie^{-i2k_R x} \\ 0 & ie^{i2k_R x} & 0 \end{pmatrix} \quad (\text{S10})$$

and $F_U^z = F_z$. Thus we have

$$\begin{aligned}\varepsilon_s &= \frac{g_2}{2} \frac{1}{V} \int dx \left[(|\psi_{+1}|^2 - |\psi_{-1}|^2)^2 + 2|\psi_0^* \psi_{+1} e^{-i2k_R x} + \psi_{-1}^* \psi_0 e^{i2k_R x}|^2 \right] \\ &= \bar{n} \frac{g_2 \bar{n}}{2} \{2|c_1 c_2|^2 \cos^2(\theta_1) \cos^2(\theta_2) \cos^2(\phi_1 + \phi_2) + |c_1 c_2|^2 \sin(2\theta_1) \sin(2\theta_2) \cos(\phi_1 - \phi_2) \\ &\quad + \left[\sum_i |c_i|^2 \cos^2(\theta_i) \cos(2\phi_i) \right]^2 + 2 \left[\sum_i |c_i|^2 \sin^2(\theta_i) \right] \left[\sum_i |c_i|^2 \cos^2(\theta_i) \right] \\ &\quad + 2\delta_{k_1, k_2-2} |c_1 c_2|^2 \sin^2(\theta_1) \cos^2(\theta_2) \sin(2\phi_2) \cos(2\alpha)\}.\end{aligned}\quad (\text{S11})$$

Then we obtain the total energy density as

$$\varepsilon = \varepsilon_0 + \varepsilon_d + \varepsilon_s. \quad (\text{S12})$$

The stripe phase is supposed to lower the spin-interaction energy density ε_s , in which there exists a term proportional to δ_{k_1, k_2-2} . This gives the mathematic reason why we always have $k_2 - k_1 = 2$ in the stripe phases.

Perturbation analysis

We consider the regime where Ω and Δ are small, and the interactions are weak. For the ground state properties, we can omit the high-energy top band safely, and consider only the two lower bands. The middle band has a minimum at $k = 2$ with spin state

$$\chi_m = \left(\frac{1}{\sqrt{2}}, 0, \frac{-1}{\sqrt{2}} \right)^T. \quad (\text{S13})$$

The bottom band has two minima, one at $k \simeq 0$ with spin state

$$\chi_{b,l} = \left(-\frac{\Omega}{4}, 1 - \frac{\Omega^2}{16}, -\frac{\Omega}{4} \right)^T, \quad (\text{S14})$$

and the other at $k \simeq 2$ with spin state

$$\chi_{b,r} = \left(\frac{1 - \frac{\Omega^2}{16}}{\sqrt{2}}, -\frac{\Omega}{2\sqrt{2}}, \frac{1 - \frac{\Omega^2}{16}}{\sqrt{2}} \right)^T. \quad (\text{S15})$$

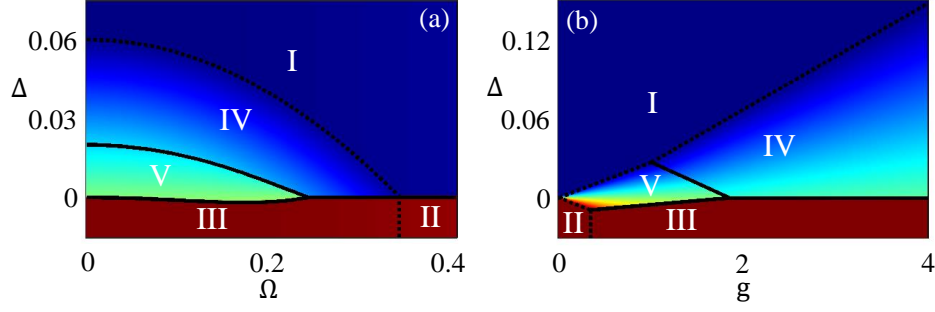


FIG. S1: (a) Phase diagram in the Ω - Δ plane with $g = 1.5$. (b) Phase diagram in the Δ - g plane with $\Omega = 0.16$. Solid lines represent first order phase transitions while dotted lines represent second order phase transitions. The phase diagram is obtained using perturbation analysis with interaction ratio $g_0 = -50g_2 \equiv g$.

As we discussed above, the ground state may contain two plane waves at most, so we consider a perturbation ansatz

$$\Psi_p = |c_1|\chi_{b,l}e^{ik_1x} + (|c_2|\chi_{b,r}e^{i\alpha} + |c_3|\chi_m e^{i\beta})e^{i(k_1+2)x}, \quad (\text{S16})$$

the energy density now becomes

$$\begin{aligned} \varepsilon = & -|c_1|^2 \frac{\Omega^2}{2} + |c_2|^2 \left(\Delta - \frac{\Omega^2}{2} \right) + |c_3|^2 \Delta + \frac{g_0}{2} (1 + |c_1|^2 |c_2|^2 \Omega^2) \\ & + g_2 [|c_1|^2 (|c_2|^2 + |c_3|^2) + 2|c_2 c_3|^2 \cos^2(\alpha - \beta)] + g_2 [|c_1 c_2|^2 \cos(2\alpha) - |c_1 c_3|^2 \cos(2\beta)] \end{aligned} \quad (\text{S17})$$

According to the second partial derivative test, it can be proven that the minima of ε always satisfy $c_1 c_2 c_3 = 0$, which means that the co-occupation of three band minima is never energetically favorable. So there are three cases:

(1) $c_1 = 0$, Ψ_p describes a plane-wave state in phase (II) or a polarized plane-wave state in phase (III), with its energy density

$$\varepsilon_{23} \equiv \varepsilon|_{c_1=0} = |c_2|^2 \left(\Delta - \frac{\Omega^2}{2} \right) + |c_3|^2 \Delta + \frac{g_0}{2} + 2g_2 |c_2 c_3|^2 \cos^2(\alpha - \beta). \quad (\text{S18})$$

(2) $c_2 = 0$, Ψ_p describes a plane-wave state in phase (I) or stripe state in phase (IV) with energy density

$$\varepsilon_{31} \equiv \varepsilon|_{c_2=0} = -|c_1|^2 \frac{\Omega^2}{2} + |c_3|^2 \Delta + \frac{g_0}{2} + 2g_2 |c_1 c_3|^2 \sin^2(\beta). \quad (\text{S19})$$

(3) $c_3 = 0$, Ψ_p describes a plane-wave state in phase (I) or stripe state in phase (V) with energy density

$$\varepsilon_{12} \equiv \varepsilon|_{c_3=0} = -|c_1|^2 \frac{\Omega^2}{2} + |c_2|^2 \left(\Delta - \frac{\Omega^2}{2} \right) + \frac{g_0}{2} (1 + |c_1|^2 |c_2|^2 \Omega^2) + 2g_2 |c_1 c_2|^2 \cos^2(\alpha). \quad (\text{S20})$$

Therefore, the ground state is determined by minimizing $\varepsilon_{12}, \varepsilon_{23}, \varepsilon_{31}$, with ground-state energy density given by $\varepsilon_g = \min\{\varepsilon_{12}, \varepsilon_{23}, \varepsilon_{31}\}$. Using Eqs. (S18), (S19), (S20), it is straight forward to calculate the ground state and the corresponding energy density ε_g . The phase boundaries can be obtained by examining the ground state or the derivation of ε_g over Ω, Δ, \dots . As shown in Figs. S1 (a) (b), we find that the phase boundary between (I) and (II) [(III) and (IV)] is $\Delta = 0$, the phase boundary between (I) and (IV) is $\Delta = -2g_2 - \Omega^2/2$, the boundary between (II) and (III) is $\Omega^2 = -4g_2$, and the boundary between (V) and (I) [(II)] is $\pm\Delta = 2g_2 + g_0\Omega/2$. The phase diagrams by perturbation analysis, as well as the behavior of the multicriticalities, are qualitatively in good agreement with the full variational calculation, though the exact phase boundaries are slightly different. This is because the perturbation results are valid only to the order of (g_2, Δ, Ω^2) , and generally the spin states of interacting BECs are slightly different from the spin states in the perturbation ansatz.

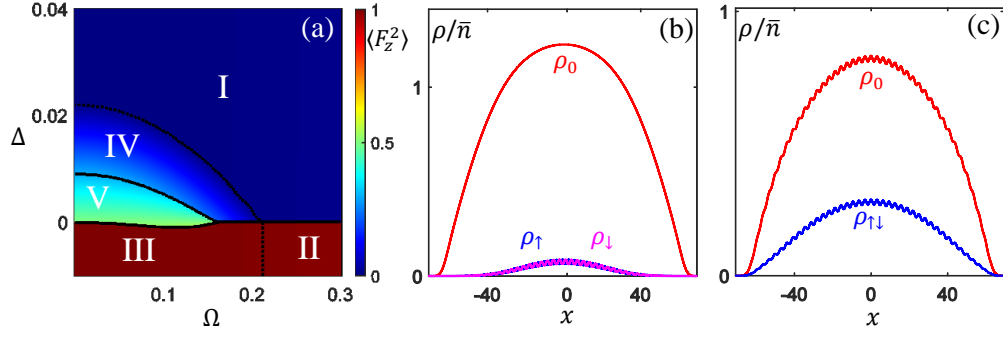


FIG. S2: (a) Ground state phase diagram in the Ω - Δ plane for ^{87}Rb BECs. Solid lines represent first order phase transitions while dotted lines represent second order phase transitions. (b) Density modulations of stripe phase (IV) in the presence of harmonic trap, with $\Omega = 0.08$, $\Delta = 0.02$. (c) Density modulations of stripe phase (IV) in the presence of harmonic trap, with $\Omega = 0.08$, $\Delta = 0.005$. In (a-c), typical ^{87}Rb interaction ratio $g_0 = -200g_2$ is used, with $g_0\bar{n} = 2.2$.

Effects of interaction ratio and harmonic trap

In the main text, we have fixed the interaction ratio as $g_0 = -50g_2$, a stronger (weaker) g_2 will enlarge (shrink) the regions of stripe and polarized plane-wave phases, but does not qualitatively change the phase diagram structure. To show this, in Fig. S2(a), we give the phase diagrams of interaction ratio $g_0 = -200g_2$ for ^{87}Rb atoms. Typically, the atomic density is about 10^{15}cm^{-3} , for s-wave scattering length $100.48a_0$ (a_0 is the Bohr radius) and Raman-laser wavelength 800nm, the corresponding interaction is $g_0\bar{n} = 2.2$. Moreover, for realistic experiments, the BECs are confined by a harmonic trap, we consider a trapping frequency $\omega = 2\pi \times 0.2\text{kHz}$ and calculate the ground state using imaginary time evolution of the GP equation. Figs. S2 (b) and (c) show the ground-state density modulations corresponding to stripe phases (IV) and (V).

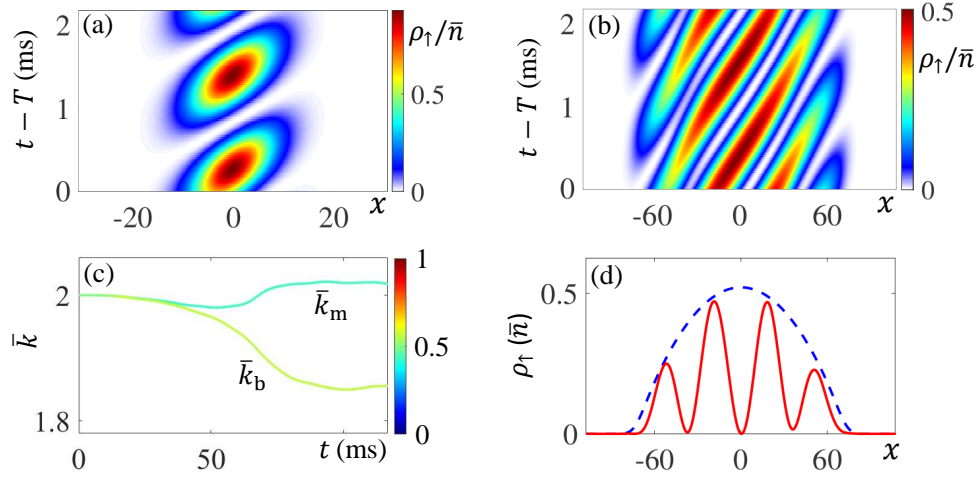


FIG. S3: (a) and (b) The evolution of the spin density corresponding to Figs. 4(d) and (e) in the main text. (c) and (d) The same as in Figs. 4(b) and (e) in the main text except that the interaction ratio of ^{87}Rb ($g_0 = -200g_2$) is used, with $g_0\bar{n} = 0.5$.

Dynamical stripe states

For the dynamical stripe states, the stripe pattern is moving rather than stationary due to the dynamical phases of the two bands, as shown in Figs. S3 (a) and (b). The long-period and high-visibility dynamical stripe states can always be obtained as long as the spin interaction is weak, as shown in Figs. S3 (c) and (d), where we consider the weakly interacting ^{87}Rb atoms with $g_0\bar{n} = 0.5$ and typical interaction ratio $g_0 = -200g_2$. The population percentage of the bottom band is slightly increased since some middle-band atoms are scattered to the bottom band by spin

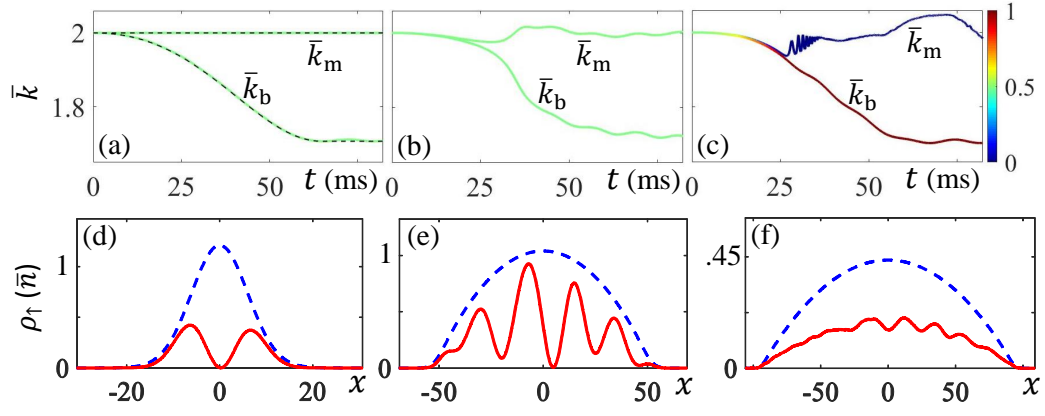


FIG. S4: (a)-(c) Averaged momentum \bar{k}_m (\bar{k}_b) and percentage population (colorbar) of atoms in the middle (bottom) band. Thin dashed line in (a) shows the band minima. (d)-(f) The initial (dashed line) and final (solid line) spin density ρ_{\uparrow} corresponding to (a)-(c) respectively. The interactions are $(g_0\tilde{n}, g_2\tilde{n}) = (0, 0)$, $(0.5, 0)$ and $(4, -0.2)$ for (a), (b) and (c). The final value of Ω is $\Omega_f = 1$, leading to a stripe period of $\sim 3\mu\text{m}$. $\omega = 2\pi \times 100\text{Hz}$ is used to reduce the time period with $T = 65\text{ms}$. The detuning is $\Delta = -0.05$.

interaction, and the stripe pattern in Fig. S3 (d) moves similarly as in Fig. S3 (b). Moreover, the modulation period can be tuned by changing the value of Ω_f , as shown in Fig. S4 with $\Omega_f = 1$ and a corresponding stripe period of $\sim 3\mu\text{m}$. In Fig. S4 (e), the stripe visibility is slightly reduced, because the spin component $|0\rangle$ in the bottom band increases slightly with Ω_f .